Contrib Mineral Petrol (2005) 150: 319–334
DOI 10.1007/s00410-005-0016-9

ORIGINAL PAPER

M. Stimpfl · J. Ganguly · G. Molin

Kinetics of Fe^{2+}–Mg order–disorder in orthopyroxene: experimental studies and applications to cooling rates of rocks

Received: 14 January 2005 / Accepted: 6 July 2005 / Published online: 7 September 2005

Abstract We determined the forward rate constant (K^+) for the Fe^{2+}–Mg order–disorder between the M2 and M1 sites of orthopyroxene (OPx), which is described by the homogeneous reaction Fe^{2+} (M2) + Mg(M1) ↔ Mg(M2) + Fe^{2+} (M1), by both ordering and disordering experiments at isothermal condition and also by continuous cooling experiments. The rate constant was determined as a function of temperature in the range of 550–750°C, oxygen fugacity between quartz–fayalite–iron and Ni–NiO buffers, and at compositions of 16 and 50 mol% ferrosilite component. The K^+ value derived from disordering experiment was found to be larger than that derived from ordering experiment at 550°C, while at $T > 580°C$, these two values are essentially the same. The fO_2 dependence of the rate constant can be described by the relation $K^+ \propto (fO_2)^n$ with $n = 5.5–6.5$, which is compatible with the theoretically expected relation. The Arrhenius relation at the WI buffer condition is given by

$$\ln(C_oK^+) = -\frac{41511 - 12600X_{Fe}}{T(K)} + 28.26 + 5.27\ X_{Fe},\ \mathrm{min}^{-1}$$

where C_o represents the total number of M2 + M1 sites occupied by Fe^{2+} and Mg per unit volume of the crystal. The above relation can be used to calculate the cooling rates of natural OPx crystals around the closure temperature (T_c) of Fe–Mg ordering, which are usually below 300°C for slowly cooled rocks. We determined the Fe–Mg ordering states of several OPx crystals (~ Fs_{50}) from the Central Gneissic Complex (Khtada Lake), British Columbia, which yields T_c ~290°C. Numerical simulation of the change of Fe^{2+}-Mg ordering in OPx as a function of temperature using the above expression of rate constant and a non-linear cooling model yields quenched values of ordering states that are in agreement with the observed values for cooling rates of 11–17°C/Myr below 300°C. The inferred cooling rate is in agreement with the available geochronological constraints.

Editorial responsibility Timothy L. Grove

M. Stimpfl
Lunar and Planetary Laboratory, University of Arizona,
Tucson, AZ 85721, USA
E-mail: mstimpfl@lpl.arizona.edu

J. Ganguly (✉)
Department of Geosciences, University of Arizona,
Tucson, AZ 85721, USA
E-mail: ganguly@geo.arizona.edu

G. Molin
Dipartimento di Mineralogia e Petrografia,
Universita' di Padova
35137, Padova, Italy
E-mail: gianmario.molin@unipd.it

Introduction

Ghose (1962) discovered that in orthopyroxene, Fe^{2+} and Mg fractionate between two nonequivalent crystallographic sites, M1 and M2, with Fe^{2+} preferring the larger site M2. The fractionation decreases with increasing temperature, but unlike metallic systems, it is a non-convergent process in that the two nonequivalent sites never become identical. Mueller (1967, 1969) recognized the potential of intracrystalline Fe–Mg fractionation in minerals as quantitative recorder of thermal history of rocks and developed the kinetic formulation to treat the process of non-convergent disordering within the framework of absolute reaction rate theory. This work was later extended by others, especially Ganguly (1982) and Sha and Chappel (1996).

During cooling, an orthopyroxene crystal undergoes ordering, but as the temperature falls below a threshold limit that depends on the cooling rate and the kinetics of ordering process, the rate of ordering becomes too slow to significantly affect the ordering state any further. This quenched ordering state preserves the memory of cooling rate near the quenching or closure temperature, T_C, and may, thus, be used to retrieve the cooling rate if the appropriate kinetic data are available. Since orthopyroxene is a widely distributed mineral in terrestrial and planetary samples, this method of retrieval of cooling rate has widespread applications, and has been applied by a number of workers to both terrestrial and planetary samples (e.g. Ganguly 1982; Anovitz et al. 1988; Skogby 1992; Ganguly and Domeneghetti 1996; e.g. Ganguly et al. 1994; Zema et al. 1997; Heinemann et al. 2000; Ganguly and Stimpfl 2000).

The kinetics of Fe–Mg order–disorder in orthopyroxene was investigated earlier by several workers (Besancon 1981; Anovitz et al. 1988; Saxena et al. 1987, 1989; Sykes-Nord and Molin 1993; Skogby 1992). However, as discussed by Ganguly and Tazzoli (1994), some of the earlier kinetic data were obtained without appropriate control of fO_2. Also, so far there has not been any investigation of the effect of fO_2 on the kinetics of Fe–Mg order–disorder even though a significant effect of fO_2 is expected on theoretical grounds (Ganguly and Tazzoli 1994). The purpose of the present study is to reinvestigate the Fe^{2+}–Mg order–disorder kinetics in orthopyroxene as function of temperature, fO_2 and composition of the crystal.

The intra-crystalline cation distribution in orthopyroxene has been determined primarily by Mössbauer Spectroscopy and structure refinement using single crystal X-ray diffraction (XRD) data. However, in recent years the latter method has been used more widely than Mössbauer Spectroscopy. This shift in technique is probably due to the greater availability of diffractometers compared to Mössbauer spectrometers, and the much smaller sample size required for XRD studies, which is a great advantage when dealing with planetary samples. Inter-comparison study of the two methods (Skogby et al. 1992) show very good agreement for Al-poor samples with intermediate iron content, when the Mössbauer data are corrected for the effect of sample thickness. However, for the relatively Al-rich and Fe-poor samples, XRD seems to give more ordered Fe–Mg distribution than Mössbauer Spectroscopy. In order to avoid the effect of technique bias, it seems desirable to use the same technique for analyzing both experimental and natural samples.

Order–disorder kinetics: theoretical background

Kroll (2003) has reviewed the different formulations of order–disorder kinetic theory in minerals that are due to Mueller (1967, 1969), Sha and Chappell (1996) and an adaptation of Ginzberg–Landau theory by Marais and Salje (1991). He showed that the Sha and Chappell theory is equivalent to the more popular Mueller theory when the system is close to equilibrium. Also the Ginzberg–Landau formalism is equivalent to Mueller theory when the average distance of cation exchange is small compared to that over which it is correlated via strain, and fluctuations of order parameter can be ignored.

In this work, we used the formulation of Mueller (1967, 1969) who treated the intracrystalline ordering of Fe^{2+} and Mg in orthopyroxene in terms of a homogeneous exchange reaction

$$\mathrm{Fe(M2)} + \mathrm{Mg(M1)} \underset{\leftarrow K^-}{\overset{K^+\rightarrow}{\leftrightarrow}} \mathrm{Fe(M1)} + \mathrm{Mg(M2)}, \qquad \text{(a)}$$

where K^+ and K^- are the specific rate constants for the forward and backward reactions, respectively. Mueller derived a rate equation by assuming that the exchange process constitutes an elementary step and obeys a second-order rate law. Integration of the rate equation yields an expression that relates the extent of change of site or sublattice composition of a binary solid solution to the time lapse under isothermal condition. Using the atomic fraction of Fe^{2+} in the M2 site, $X_{\mathrm{Fe}}^{\mathrm{M2}}$, as the monitor of change of the sublattice composition, Mueller's integrated expression can be written as

$$-(C_o\mathrm{K}^+)\Delta t = \frac{1}{(b^2-4ac)^{1/2}} \times \left[\ln\left|\frac{\left(2aX_{\mathrm{Fe}}^{\mathrm{M2}}+b\right)-\left(b^2-4ac\right)^{1/2}}{\left(2aX_{\mathrm{Fe}}^{\mathrm{M2}}+b\right)+\left(b^2-4ac\right)^{1/2}}\right|\right]_{X_{\mathrm{Fe}}^{\mathrm{M2}}(t_o)}^{X_{\mathrm{Fe}}^{\mathrm{M2}}(t)}, \qquad (1)$$

where a, b and c are constants at a give temperature and pressure, and C_o is the number density of the sites (that is the total number of sites per unit volume of the crystal) involved in the exchange reaction. C_o is nearly a constant term, and is usually absorbed in the rate constant. The constants a, b and c depend on k_D and the bulk composition of the crystal. If X_{Fe} is bulk atomic fraction of Fe and p and q are the site fractions of M2 and M1, respectively, then

$$\begin{aligned} X_{\mathrm{Fe}} &= p\left(X_{\mathrm{Fe}}^{\mathrm{M2}}\right) + q\left(X_{\mathrm{Fe}}^{\mathrm{M1}}\right) \\ &= p\left(X_{\mathrm{Fe}}^{\mathrm{M2}}\right) + (1-p)\left(X_{\mathrm{Fe}}^{\mathrm{M1}}\right). \end{aligned} \qquad (2)$$

In Eq. 1 the backward rate constant, K^-, is eliminated by the relation $k_D = \mathrm{K}^+/\mathrm{K}^-$, which holds if the cation exchange reaction constitutes an elementary step. Here k_D is the intracrystalline distribution coefficient that is defined as

$$k_D = \frac{(\mathrm{Fe/Mg})^{\mathrm{M1}}}{(\mathrm{Fe/Mg})^{\mathrm{M2}}}. \qquad (3)$$

Here and elsewhere Fe stands for Fe^{2+}, unless stated otherwise. Within the argument of the logarithmic term in Eq. 1, the numerator is positive for an ordering process and negative for a disordering process, and hence the modulus sign for the argument.

Using Eq. 1, the forward rate constant, K^+, can be determined by isothermal time series experiments leading to either progressive ordering or progressive disordering as a function of time. We would designate K^+

derived from the two types of experiments as K^+ (ord) and K^+ (disord), respectively. It is customary to cast the rate constant derived at different temperatures in the form of an Arrhenian relation as

$$\ln(C_o K^+) = \ln(C_o K_o) - \frac{Q}{RT}, \tag{4}$$

where Q is the activation energy, R is the gas constant and K_o, which has the dimension of t^{-1}, is a constant at constant state conditions and bulk composition of the crystal.

Since order–disorder kinetics is a diffusion controlled process, which depends on the concentration of point defects, and fO_2 conditions affect the latter by the homogeneous oxidation–reduction reaction of heterovalent element like Fe, it is expected that the kinetics of Fe–Mg order–disorder process would be affected by fO_2 in much the same way as a diffusion process. To a very good approximation, the Fe–Mg interdiffusion coefficient, D(Fe–Mg), varies as $(fO_2)^{1/6}$ (Buening and Buseck 1973; Meisner 1974; Morioka and Nagasawa 1991). This behavior is not structure specific, but reflects the effect of fO_2 on concentration of point defects by redox reaction of iron. Thus, we expect that the rate constant for the Fe–Mg order–disorder process in orthopyroxene to have ~1/6 power dependence on fO_2.

Previous studies

The kinetics of Fe–Mg order–disorder in orthopyroxene has been studied by a number of earlier workers using single crystal X-ray diffraction (Saxena et al. 1987, 1989; Sykes-Nord and Molin 1993; Ganguly and Stimpfl 2000) and Mössbauer Spectroscopy (Besancon 1981; Anovitz et al. 1988; Skogby 1992) to determine the site occupancies of the cations. Ganguly and Tazzoli (1994) presented an optimized expression for the rate constant K^+ as a function of T and X at fO_2 of ~0.8 log unit above the wüstite-iron (WI) buffer. They used only the data of Besancon (1981) and Anovitz et al. (1988) since these were the only experiments that were conducted at controlled fO_2 conditions prior to their study. The calibration of Ganguly and Tazzoli (1994) has been used to retrieve cooling rates for host rocks on the basis of ordering state of natural orthopyroxenes (Zema et al. 1997; Heinemann et al. 2000). However, upon a thorough review of the available kinetic data, Kroll et al. (1997) found some inconsistencies in the values of rate constants derived by Besancon (1981) and Anovitz et al. (1988) and thus recalculated the rate constants from their experimental data.

Ganguly and Stimpfl (2000) carried out continuous cooling experiments at fO_2 conditions corresponding to those of wüstite–iron (WI) buffer, and retrieved the Arrhenian parameters of the rate constant, K^+ (ord), for a nearly binary Fe–Mg orthopyroxene with $X_{Fe} = 0.16$ (or Fs_{16}). They used XRD technique and a single crystal point (or serial) diffractometer to determine the site occupancies after each experiment. Their calibration is about two orders of magnitude slower than that derived from the expression of Ganguly and Tazzoli (1994) for the same composition.

Experimental studies

We conducted a series of kinetic experiments as a function of temperature, using orthopyroxenes of two different compositions (Fs_{16} and Fs_{50}) and different fO_2 conditions. The kinetic experiments involved two different approaches, namely (a) isothermal time series experiments and (b) continuous cooling experiments. Site occupancies were determined by means of single crystal X-ray diffractions and structural refinements using the bulk chemical constraints. The chemical composition for each crystal was determined by electron microprobe analysis after completion of all kinetic experiments on the crystal.

Starting material

A low-Fe sample (Fs_{16}), labelled ST5, was separated from the stony iron meteorite Steinbach while orthopyroxene crystals with X_{Fe} ~0.50 (Fs_{50}) were separated from a granulite facies sample from the Khtada Lake Metamorphic Complex within the Central Gneiss Complex (CGC), British Columbia, Canada (Hollister 1982; sample TPR-30F). These orthopyroxene samples were labeled HOY, where Y is a variable reference number. Of the samples used in this study, sample ST5 was previously used to determine the kinetic constants by continuous cooling experiments by Ganguly and Stimpfl (2000) and the sample HO28 was used to determine the equilibrium fractionation of Fe–Mg by Stimpfl et al. (1999).

It was shown by Zema et al. (1999) and Heinemann et al. (2000) in two independent studies of samples from the Johnstown meteorite that the presence of exsolution texture has a strong effect on Fe–Mg order–disorder kinetics. Càmara et al. (2000) carried out TEM analysis of the microstructures of an orthopyroxene crystal from the CGC, British Columbia, that was provided by us from the same stock of material used in this study. No exsolution texture or Guinier–Preston zones were detected in this sample.

Electron microprobe analyses

Elemental compositions of all crystals, except ST5 and HO28, were calculated in this study by averaging a large number of spot analyses (80–100) determined by a CAMECA SX50 electron microprobe (EMP) with wavelength dispersive spectrometers (WDS), using

15 kV accelerating voltage, 20 nA beam current and 30 s counting times for both peak and background measurements. Abundance of the elements Si, Ca, Ti, Cr, Al, Mn, Na, Mg, and Fe, were calculated using the following standards: synthetic diopside for Si and Ca, ilmenite for Ti, synthetic chromite for Cr, synthetic pyrope for Al, synthetic spessartine for Mn, natural albite for Na, synthetic enstatite for Mg, and synthetic ferrosilite for Fe. All specimens used were found to be homogeneous within the resolution of the microprobe. The compositions for ST5 and HO28 were previously determined by Ganguly and Stimpfl (2000) and Stimpfl et al. (1999), respectively. All iron was assumed to be Fe^{2+}. For the sample ST this assumption is justified by the fact that it is derived from a stony-iron meteorite, Steinbach, which had fO_2 condition within the field of metallic iron. On the other hand, a Mössbauer study of orthopyroxenes taken from the same stock from which the HO28 crystal was separated showed no Fe^{3+} within the detection limit, ≥ 1%, of this technique (Hans Annersten, personal communication).

The average elemental compositions of each crystal along with their respective standard deviations were used to determine its statistically most-probable bulk composition. This was achieved by projecting the average composition of each element, weighted by its respective variance, on the *n*-dimensional surface that satisfies the crystal chemical constraints for orthopyroxene (Dollase and Newman 1984; Stimpfl et al. 1999). Usually, the adjusted composition for each element was within 1 standard deviation ($\pm 1\sigma$) of its average composition. The average and adjusted compositions of all samples are summarized in Table 1.

Kinetic experiments

For the kinetic experiments, the sample was contained in a small gold capsule and was placed on top of another gold capsule containing a solid fO_2 buffer mixture, both capsules being sealed at the lower end. The double capsule assembly was usually sealed within a SiO_2 tube. The buffer mixture consisted of either wüstite plus iron (WI) or Ni plus NiO (NNO). We emphasize at the outset, and as would be evident later, that the presence of a buffer mixture in a sealed silica tube did not ensure that the fO_2 within the tube was necessarily controlled by that of the buffer mixture. This is a point that we did not appreciate until our experimental studies started showing results that were mutually incompatible. Also, it was not clear to us in the beginning how much time was needed to equilibrate the point defects in the crystal to the imposed fO_2 condition at different temperatures. The mutual inconsistencies of the results that were the consequence of discontinuous variation of fO_2 condition within a silica tube from the fO_2 of WI buffer to that of quartz–fayalite–iron (QFI) buffer, and also the lack of equilibration of point defects at temperature at or below 580°C, as became evident from the results of the experiments, prompted us to carry out additional experiments with different approaches. The modified experimental protocol, which will be described later, involved three samples, HO11-108, ST5-113, HO11-109.

The charge was placed into a preheated oven and drop quenched in cold water after annealing for a desired length of time. Temperature was controlled by a computer and monitored by a Pt-10%Rh thermocouple placed beside the charge for all experiments, and recorded into a file at regular intervals by the computer. After each experiment, the ordering state of the annealed crystal was determined by XRD and structure refinement. The buffers were checked at the end of most experiments by means of X-ray powder diffraction to confirm the presence of both phases. Because of severe sintering of the WI mixture during an experiment, it proved too difficult to grind some of the mixtures for the purpose of powder X-ray diffraction.

For the isothermal experiments, an experimental charge was placed in a preheated oven for a period shorter than that required to achieve the equilibrium ordering state. After quenching and X-ray data collection, the sample was again annealed at the same temperature. This procedure was repeated until the site occupancies reached a steady-state value. We conducted both ordering and disordering experiments at several temperatures in the range 550–750°C. The fO_2 buffer mixture consisted of wüstite plus iron for the experiments at 550, 650 and 750°C. The experiments at 580°C were conducted separately with two types of buffer mixtures, WI and NNO. The experimental conditions and results are summarized in Table 2.

For continuous cooling experiments a crystal was first annealed at a fixed temperature for sufficiently long time for it to achieve equilibrium and was then subjected to cooling that was controlled by a computer. After each experiment we analyzed the T–t data and were able to fit either linear or an exponential cooling curve to the data, according to $T = T_o - \beta t$ or $T = T_o \exp(-\alpha t)$, where β and α are constants with dimensions of Kt^{-1} and t^{-1} respectively. The experimental conditions and results of continuous cooling experiments are summarized in Table 3. Isothermal experiments were conducted only with the HO samples while continuous cooling experiments were conducted with both HO (Fs_{50}) and ST(Fs_{16}) samples.

X-ray data collection and structure refinements

Single crystal X-ray intensity data were collected after each annealing experiment using either a conventional four-circle point-detector diffractometer (PD) or a modern area detector diffractometer equipped with charge-coupled device (CCD). The data collection and reduction procedures in these two types of diffractometers are described below.

In the PD, equivalent pairs hkl and $h\bar{k}l$ were measured using ω scan mode in the θ range 1.5° to 30° or 35°. The PD-s used in this study were AED II and

Table 1 Initial (i.e., measured) and adjusted (adj) compositions of the orthopyroxene crystals used for the kinetic experiments

Sample	ST5	Esd[a]	ST5adj	HO8	Esd	HO8(adj)	HO10	Esd	HO10(adj)	HO11	Esd	HO11(adj)	HO13	Esd	HO13(adj)
XFe			0.159			0.502			0.499			0.496			0.498
Si	1.994	(6)	1.989	1.971	(4)	1.977	1.973	(4)	1.975	1.975	(5)	1.974	1.973	(3)	1.976
Al	0.012	(1)	0.011	0.036	(4)	0.038	0.043	(3)	0.044	0.045	(2)	0.045	0.039	(4)	0.042
Ti	0.001	(1)	0.001	0.004	(1)	0.004	0.003	(1)	0.003	0.003	(1)	0.003	0.003	(1)	0.003
Cr	0.012	(1)	0.012	0.000	(1)	0.000	0.000	(1)	0.000	0.000	(1)	0.000	0.000	(1)	0.000
Mg	1.641	(9)	1.647	0.977	(4)	0.973	0.971	(7)	0.968	0.971	(3)	0.972	0.971	(3)	0.968
Fe^{2+}	0.309	(5)	0.311	0.965	(6)	0.954	0.968	(8)	0.964	0.955	(5)	0.956	0.966	(4)	0.960
Mn	0.016	(1)	0.016	0.015	(1)	0.015	0.015	(1)	0.015	0.014	(1)	0.014	0.015	(1)	0.015
Ca	0.012	(1)	0.012	0.038	(1)	0.038	0.031	(1)	0.031	0.034	(1)	0.034	0.035	(1)	0.036
Na	0.001	(1)	0.001	0.002	(1)	0.001	0.001	(1)	0.000	0.001	(1)	0.001	0.001	(1)	0.000
Total	3.998		4.000	4.008		4.000	4.004		4.000	3.999		4.000	4.004		4.000
Charge	12.009		12.000	12.000		12.000	12.000		12.000	12.000		12.000	12.000		12.000
Al(T)[b]	0.006		0.011	0.029		0.023	0.027		0.025	0.025		0.026	0.027		0.024
Al(M)[b]	0.006		0.000	0.007		0.015	0.015		0.020	0.021		0.020	0.012		0.018
d(chrg(M)[c]	0.019		0.011	0.013		0.023	0.020		0.025	0.027		0.026	0.018		0.024
d(M-T)[d]	0.013		0.000	−0.016		0.000	−0.007		0.000	0.002		0.000	−0.009		0.000
M-cations	1.998		2.000	1.999		2.000	2.004		2.000	1.999		2.000	2.004		2.000

Sample	HO14	Esd[a]	HO14(adj)	HO15	Esd	HO15(adj)	HO28	Esd	HO28(adj)	HO39B	Esd	HO39B(adj)
XFe			0.502			0.498			0.508			0.511
Si	1.970	(4)	1.974	1.973	(3)	1.976	1.970	(5)	1.975	1.979	(9)	1.981
Al	0.043	(4)	0.045	0.039	(2)	0.042	0.041	(1)	0.042	0.033	(7)	0.032
Ti	0.003	(1)	0.004	0.003	(1)	0.003	0.003	(1)	0.004	0.004	(1)	0.004
Cr	0.000	(1)	0.000	0.000	(1)	0.000	0.000	(1)	0.001	0.000	(1)	0.000
Mg	0.965	(8)	0.958	0.973	(5)	0.969	0.952	(6)	0.947	0.945	(4)	0.944
Fe^{2+}	0.971	(7)	0.966	0.964	(6)	0.959	0.988	(8)	0.979	0.990	(6)	0.988
Mn	0.015	(1)	0.014	0.015	(1)	0.015	0.014	(1)	0.014	0.016	(1)	0.015
Ca	0.038	(1)	0.038	0.035	(1)	0.035	0.038	(1)	0.038	0.036	(1)	0.036
Na	0.001	(1)	0.001	0.001	(1)	0.001	0.001	(1)	0.000	0.001	(1)	0.001
Total	4.006		4.000	4.005		4.000	4.007		4.000	4.002		4.000
Charge	12.000		12.000	12.000		12.000	12.000		12.000	12.000		12.000
Al(T)[b]	0.030		0.026	0.027		0.024	0.030		0.025	0.021		0.019
Al(M)[b]	0.013		0.019	0.012		0.018	0.010		0.017	0.011		0.012
d(chrg(M)[c]	0.019		0.026	0.018		0.024	0.016		0.025	0.018		0.019
d(M-T)[d]	−0.011		0.000	−0.008		0.000	−0.014		0.000	−0.003		0.000
M-cations	2.006		2.000	2.005		2.000	2.007		2.000	2.002		2.000

An initial composition represents the mean of 80–100 spot analyses; an adjusted composition represents the statistically most-probable bulk composition. Standard deviations from the mean are given in parenthesis in the right justified format

[a] *Esd*, estimated standard deviation from the mean of the spot analyses

[b] *Al(T)*, Al in T site; Al (M): Al in M site

[c] *d(chrg(M))*, excess positive charge in M site due to the substitution for 2^+ cations

[d] *d (M-T)*, difference between the charge excess in M site and the charge deficiency in T site

NONIUS CAD-4 that employed Mo *K*α radiation (λ = 0.71073 Å) and graphite monochromator. The X-ray intensities were corrected for Lorentz, polarization and absorption factors (North et al. 1968) and then averaged for equivalent pairs in the Laue class *mmm*. No violations were observed for the *Pbca* extinction conditions.

The data for the CCD runs were collected using a BRUKER SMART1000 diffractometer using the Mo *K*α radiation as well and a graphite monochromator. X-ray intensities were collected in the range 1.5–40° or 42°, using the Bruker SMART software package (Bruker 1997b). A total of 4,948 frames were collected for each sample, each frame having an X-ray exposure time of 10 s and consisting of ω scan of 0.15° in width. The data were collected in multirun mode in which six runs were selected to maximize randomness (0° and 90° for phi). Of these, two short runs of 50 frames were used to monitor decay of X-ray intensity.

The CCD area-detector was positioned at 5.3 mm from the crystal. All CCD data were collected at room temperature except for run HO11-101 which was collected at 110°K to evaluate if the reduction of thermal vibration leads to any significant improvement in the determination of site occupancies. After completion of the data collection, the Bruker SAINT software (Bruker 1997a) was used to integrate the observed intensities. The sharpness of the peaks allowed the use of box optimization and narrow frame algorithm as integration conditions. For all samples the results of the box optimization algorithm converged. Without imposing any crystallographic constraints, the orientation matrix was updated at intervals of 303 frames to adjust for possible crystal translations. However, none were detected. Lorentz and polarization corrections were also applied using the program SAINT of the SMART CCD package.

Table 2 Experimental conditions and observed $X_{\mathrm{Fe}}^{\mathrm{M2}}$ for isothermal experiments for HO28, HO39B, HO13, HO15, HO14 and HO8

Sample-ID	Type of experiment	T°C	Time/min	Buffer	P	XFe$^{\mathrm{M2}\ \mathrm{a}}$	Rate constant (min^{-1})	
							C_0K^+ (disord)	C_0K^+ (ord)
HO28-26	Untreated		0		0.4921	0.9000(10)		
−34	DIS	550	7200	WI		0.8200(10)		
−39	DIS	550	15840	WI		0.8109(10)		
−44	DIS	550	24480	WI		0.8052(10)		
−49	DIS	550	44640	WI		0.8012(11)		
−56	Equilibrium	550	73440	WI		0.7986(11)	3.72×10^{-5} (58)	
−67	DIS	650	300	WI		0.7679(11)		
−73	DIS	650	470	WI		0.7697(10)		
−80	DIS	650	710	WI		0.7722(10)		
−84	DIS	650	900	WI		0.7662(10)		
−87	Equilibrium	650	1800	WI		0.7667(10)	1.50×10^{-3} (1.4)	
−94	DIS	750	4	WI		0.7654(10)		
−100	DIS	750	9	WI		0.7590(10)		
−104	DIS	750	20	WI		0.7420(10)		
−107	DIS	750	40	WI		0.7433(10)		
−111	DIS	750	160	WI		0.7409(10)		
−111a	DIS	750	160	WI		0.7409(13)		
−117	DIS	750	220	WI		0.7390(11)		
−122	Equilibrium	750	310	WI		0.7389(10)	2.80×10^{-2} (54)	
−134	Equilibrium	850	840	WI		0.7134(11)		
−137	Equilibrium	750	900	WI		0.7178(11)		
−141	ORD	650	30	WI		0.7449(10)		
−142	ORD	650	75	WI		0.7432(11)		
−145	ORD	650	225	WI		0.7528(10)		
−146	ORD	650	420	WI		0.7556(12)		
−148	ORD	650	900	WI		0.7582(13)		
−151	ORD	650	1800	WI		0.7616(10)		
−152	Equilibrium	650	2700	WI		0.7650(10)		9.50×10^{-4} (3)
−153	ORD	550	21600	WI		0.7811(10)		
−155	ORD	550	47520	WI		0.7831(10)		
−156	ORD	550	83520	WI		0.7906(10)		
−158	ORD	550	122400	WI		0.7937(10)		
−160	ORD	550	158400	WI		0.7926(10)		4.70×10^{-6} (43)
HO39B-159	Equilibrium	850	480	WI	0.4911	0.7147(10)		
−161	ORD	750	4	WI		0.7235(11)		
−162	ORD	750	12	WI		0.7290(11)		
−163	ORD	750	18	WI		0.7320(10)		
−2	ORD	750	54	WI		0.7410(14)		
−4	ORD	750	340	WI		0.7412(16)		2.30×10^{-2} (20)
HO13-11	Untreated		0		0.4924	0.8913(14)		
−15	DIS	580	618	WI		0.8248(13)		
−21	DIS	580	798	WI		0.8159(14)		
−38	DIS	580	978	WI		0.8060(34)	4.56×10^{-4} (30)	
HO15-23	Untreated		0		0.4926	0.8917(11)		
−27t	DIS	580	618	NNO		0.8197(31)		
HO14-24	Equilibrium	750	94	WI	0.4923	0.7348(13)		
−27t	ORD	580	618	WI		0.7641(13)		
HO8-44a	Equilibrium	750	94	NNO	0.4923	0.7345(13)		
−46	ORD	580	620	NNO		0.7681(12)		
−49	ORD	580	809	NNO		0.7669(24)		
−50	ORD	580	978	NNO		0.7724(18)		4.36×10^{-4} (50)

Esd reflects only structural errors. The equilibrium data are from Stimpfl (2005a, b). The site occupancies of all samples were determined using a point detector diffractometer. P is the fraction of M2 sites occupied by Fe plus Mg. The numbers within the parentheses are standard deviations in the right justified format

DIS Disordering experiments; *ORD* ordering experiments

[a] XFe(M2) = nFe(M2)/(nFeM2 + nMg(M2)), n = number of moles

A total of 12,600–14,000 reflections were observed for each sample. These were integrated in the space group *Pbca* and were corrected for λ/2 factor and absorption using the program SADABS (Sheldrick 1996). Merging and averaging of equivalent reflections were performed in the Laue point group *mmm* using the program SORTAV (Blessing 1987). No violations of the *Pbca* extinction conditions were observed for any crystal. A total of ~2,500 independent reflections were generated after merging the data. Finally, unit cell parameters were refined with the constraint of orthorhombic symmetry using Bruker SAINT software (Bruker 1997a).

Table 3 Experimental conditions and quenched $X_{\mathrm{Fe}}^{\mathrm{M2}}$ values for continuous cooling experiments

Sample-ID	Buffer	P	T_{o} (°C)	Annealing time(min)	Cooling model	Cooling constant or cooling rate	$X_{\mathrm{Fe}}^{\mathrm{M2}}$ [a]	T_{c} (°C)
HO13-57	WI		850	142	exp	0.0098	0.7162(12)	795
HO11-79	WI	0.4931	902	1303	exp	0.0060	0.7176(14)	779
HO11-98	WI		954	1337	linear	2.1700	0.7307(11)	729
HO11-118	WI		950	14400	linear	0.5000	0.7405(11)	694
HO14-60	WI		793	130	linear	0.9960	0.7428(19)	708
HO11-109	WI[b]		850	5484	linear	0.4000	0.7430(13)	685
HO11-88	WI		1002	1146	exp	0.0044	0.7152(11)	789
HO11-108	QFI		947	2820	linear	3.0000	0.7224(11)	761
HO11-101	WI[c]		904	1671	linear	0.5500	0.7356(11)	710
HO11-104	WI		904	1671	linear	0.5500	0.7349(11)	714
HO15-58	NNO		847	142	exp	0.0098	0.7336(18)	726
HO10-80t2	NNO	0.4939	902	1303	linear	3.1700	0.7440(14)	689
ST5-119	WI	0.4959	950	14400	linear	0.0500	0.2733(8)	794
ST5-113	WI[b]		942	2880	linear	0.5000	0.2678(10)	851
ST5-82	WI		750	10080	linear	0.0052	0.2794(9)	682
ST7[d]	WI	0.4961	1000	–	linear	12.27	0.2605(12)	952
ST6[d]	WI	0.4954	950	–	linear	2.4	0.2628(11)	903
ST5[d]	WI		913	–	linear	0.485	0.2674(12)	857
ST5[d]	WI		750	–	linear	0.011	0.2781(12)	745

Eds reflect only structural errors. The site occupancies for all experiments were determined using CCD equipped diffractometer except for HO13-57, HO14-60, HO15-58 and for the data of Ganguly and Stimpfl (2000) which were determined using point detector diffractometers. T_{o}, starting temperature; T_{C}, closure temperature

[a] XFe(M2) = nFe(M2)/(nFeM2 + nMg(M2); n = number of moles

[b] Silica tube substituted by gold tube

[c] Collected at 110°K; same experiment as HO11-104 which was collected at room T

[d] Intensity data from Ganguly and Stimpfl (2000); site occupancy re-determined following Stimpfl (2005)

Site occupancies were refined with the program RFINE90 (Finger and Prince 1975), using F_{o} generated from the observed F_{o}^2 by the program BAYES (Blessing 1987), ionic scattering factors, and bulk compositional constraints. The procedure for site occupancy determinations is essentially the same as in Stimpfl et al. (1999) that should be consulted for further details. The only modification is in our treatment of Mn fractionation. On the basis of the work of Hawthorne and Ito (1978), it has been the usual practice to fractionate Mn and Fe in the same way between the M1 and M2 sites, as if these constitute a single species. The same procedure was also followed by Stimpfl et al. (1999). However, new experimental data on the fractionation behavior of Mn in Donpeacorite ($Mg_{1.43}Mn_{0.54}Ca_{0.3}Si_2O_6$) show that Mn orders almost exclusively to the M2 site (Stimpfl 2005a, b). Consequently, we partitioned only Fe and kept Mn totally ordered to M2. Cell parameters, interatomic distances, final atomic parameters, observed and calculated structure factors are available from the authors. The agreement index in the structure refinement, R_{w}, were within 0.014–0.035.

Modeling and retrieval of kinetic parameters: *T*, fO$_2$ and *X* dependence

The data for intracrystalline Fe–Mg distribution coefficient, k_{D}, versus T that were needed to model the evolution of site occupancies of the samples were taken from Stimpfl (2005a, b). The calibrations for the intermediate and low iron samples, HO(Fs$_{50}$) and ST5(Fs$_{16}$), which were used in the kinetic experiments, are as follows:

$$\mathrm{HO(Fs_{50})}: \quad \ln k_{\mathrm{D}} = -\frac{2708(\pm 58)}{T(\mathrm{K})} + 0.695(\pm 0.058), \tag{5}$$

$$\mathrm{ST5(Fs_{16})}: \quad \ln k_{\mathrm{D}} = -\frac{2984(\pm 69)}{T(\mathrm{K})} + 0.747(\pm 0.078). \tag{6}$$

These equations represent minor modification of the calibration by Stimpfl et al. (1999) to account for the change of the fractionation scheme of Mn between the M2 and M1 sites, as discussed above.

Isothermal experiments

The site occupancies determined in the isothermal ordering and disordering experiments using the HO(Fs$_{50}$) samples are listed in Table 2, and illustrated as a function of time in Figs. 1 and 2. The estimated standard deviations (Esd) of the site occupancies reflect only those arising from the structural errors. A thorough analysis of the effect of uncertainties of the microprobe analyses on the Esd of the site occupancies is an involved procedure that has not yet been carried out. However, the preliminary studies of Stimpfl et al. (1999) suggest that the propagation of the uncertainties of the microprobe analyses of the samples could expand the Esd of the site occupancies by a factor of 3–4. The forward rate constant at each temperature from both ordering and disordering experiments, C_0K^+ (disord) and C_0K^+ (disord) respectively, were determined by linear

Fig. 1 a–c Isothermal evolution of X_{Fe}^{M2} as a function of time at 550°C, 650°C and 750°C for both ordering (*upright triangles*) and disordering (*downward pointing triangles*) experiments. All experiments were performed on sample HO28(Fs_{50}) with the exception of the ordering experiments at 750°C, for which we used sample HO39B (*empty triangles*). The experiments were conducted in the presence of WI buffer mixture in sealed silica tube (see text for discussion of buffer effectiveness). The *t* versus X_{Fe}^{M2} was modeled using the kinetic constants in Table 2. The symbol heights are approximately twice the standard deviation of site occupancies

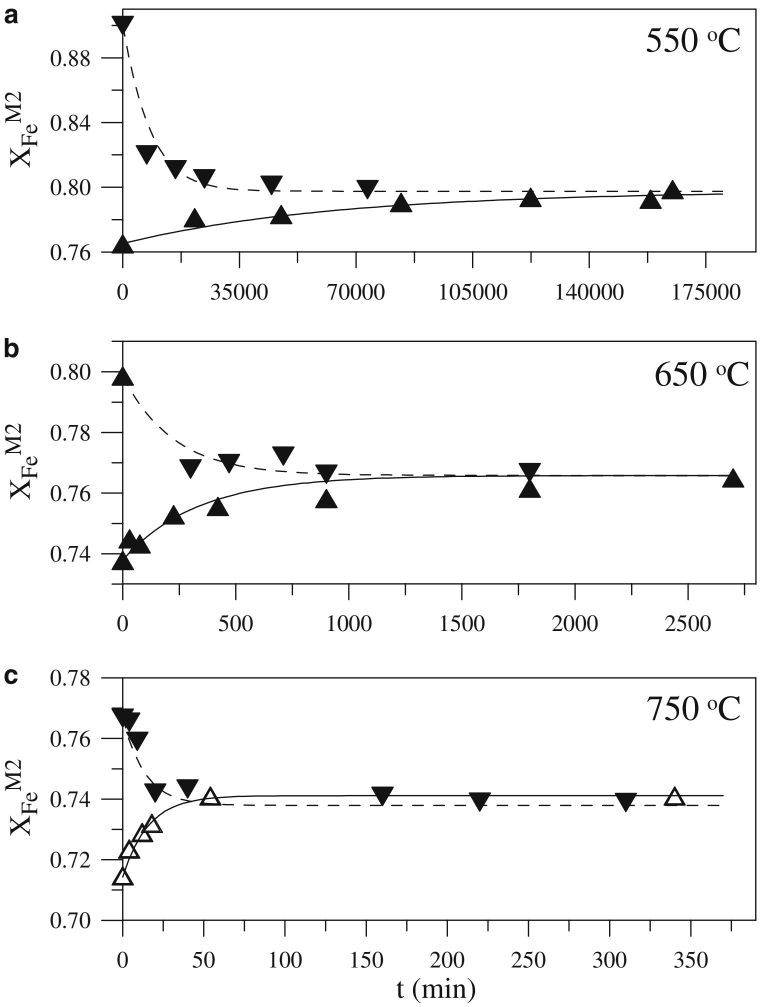

regression of the right-hand side of Eq. 1, referred to as f(M2), versus time. The regression was done by using the statistical package SPSS (12.0). Each f(M2) was weighted by the inverse of its variance.

The values of (C_0K^+) retrieved from the isothermal experimental data are summarized in Table 2. The forward rate constants derived from ordering experiments are referred to as C_oK^+ (ord) while those derived from disordering experiments are referred to as C_oK^+ (disord). The model fits to the site occupancy data as function of time using the retrieved kinetic constants are illustrated in Figs. 1 and 2. Figures 1a–c illustrate the results for isothermal experiments at 550°C, 650°C and 750°C that were conducted with WI buffer mixtures in sealed silica tube. Figure 2 illustrates the results for the samples HO13, HO14, HO15 and HO8, which were annealed at 580°C. Experiments with the first two and last two samples were carried out in the presence of WI and NNO buffer mixtures, respectively. However, despite a variation of fO_2 condition by ~5 orders of magnitude between these two buffers, all data conform to a single rate constant in either disordering or ordering experiment (Fig. 2). This insensitivity of the Fe–Mg order–disorder kinetics to large variation of fO_2 condition indicates that the point defects did not equilibrate to the imposed fO_2 condition in the experiments at 580°C.

The retrieved kinetic constants are plotted in the form of an Arrhenian relation, that is log(C_oK^+) versus $1/T$, in Fig. 3, in which the upward and downward pointing triangles indicate ordering and disordering experiments, respectively. There are two significant aspects in the data plotted in Fig. 3 that require careful analysis before these are regressed to retrieve an Arrhenian expression. (a) The data at 580°C stand out as clear outliers, and (b) the K^+ value derived from disordering experiment is significantly larger than that derived from ordering experiment at 550°C, whereas at higher temperatures, K^+ (ord) is effectively the same as K^+ (disord). Since the point defects did not equilibrate in the experiments at 580°C, we must conclude that these did not equilibrate also with the fO_2 condition of the experiments at 550°C.

All data plotted in Fig. 3, except those at 580°C, were obtained from two crystals (Table 2). Referring to the numbers beside the data symbols in Fig. 3, the natural crystal HO28 (0), which had a closure temperature (T_c)

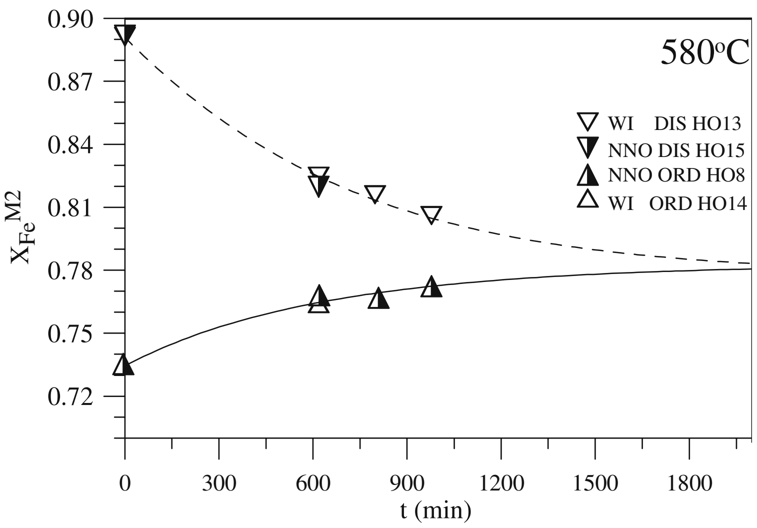

Fig. 2 Isothermal evolution of $X_{\mathrm{Fe}}^{\mathrm{M2}}$ as a function of time at 580°C for both ordering and disordering experiments (*upright triangles*: ordering experiments; *downward pointing triangles*: disordering experiments). The experiments indicated by open (HO13 and HO14) and *half-filled symbols* (HO8 and HO15) were conducted in the presence of WI and NNO mixtures, respectively, in sealed silica tubes

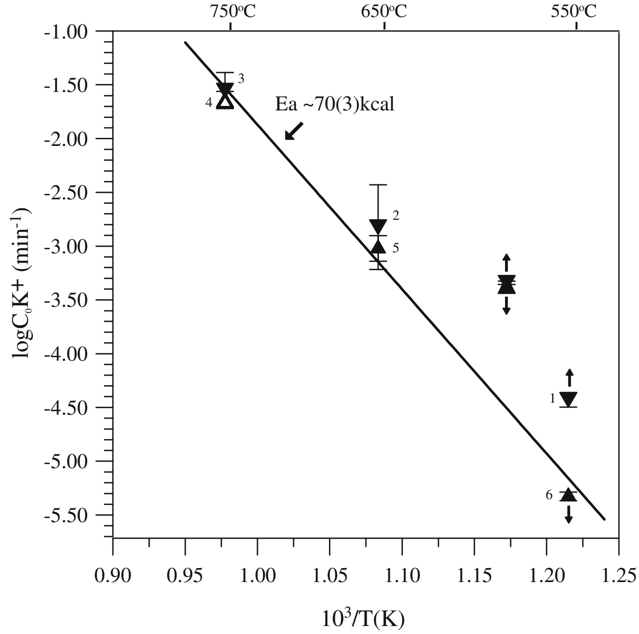

Fig. 3 Temperature dependence of log(C_oK$^+$) determined from isothermal ordering (*upright triangles*) and disordering (*downward pointing triangles*) experiments. All experiments were conducted using WI buffer mixture in sealed silica tubes except the one represented by *upward pointing triangle* at 580°C, which was conducted in the presence of NNO buffer mixture. *Filled triangles*: sample HO28, *open triangle*: sample HO39b. Except for the ordering experiment at 550°C, all data at ≤ 580°C were ignored in the regression, which is shown by a *solid line*. The *error bars* on the data points represent ±1σ. The upward and downward pointing arrows on the data points at 580°C and 550°C indicate possible displacements of the data had point defect equilibrium been achieved at these temperatures

for Fe–Mg ordering of ~ 300°C (see later), was annealed at different *T*–fO$_2$ conditions of the WI buffer in the sequence 0 → 1 → 2 → 3 → 850°C → 5 → 6, while the sample HO39B was annealed according to the sequence 0 → 850°C → 4. Since the point defects did not equilibrate in the experiments at 580°C, and the sample used for the ordering experiment at this temperature was pre-annealed at 750°C (Table 2), the ordering kinetics at 580°C must have been somewhat overestimated because of the presence of larger than the equilibrium point defect concentrations. On the other hand, the disordering kinetics at both 580°C and 550°C (#1) were most likely underestimated since the orthopyroxene crystal was separated from a granulite (CCG, British Columbia), and the fO$_2$ of a granulite at ~300°C (i.e., T_c), which must have been within a few orders of magnitude of the that defined by the quartz–fayalite–magnetite buffer, was much lower than that of WI buffer at 550°C. Thus, we conclude that at 550°C, K$^+$(ord) < K$^+$(disord). The expected directions of displacements of the K$^+$(ord) and K$^+$(disord) data at 580°C and 550°C, had point defect equilibrium been achieved, are shown by arrows in Fig. 3.

In their study of Fe–Mg order–disorder kinetics of anthophyllite at 500°C and 550°C, Seifert and Virgo (1973) found that K$^+$(ord) < K$^+$(disord). Later, O'Neill (1994) found the Fe–Mg disordering kinetics in spinel to be faster than the ordering kinetics in the temperature range of 553–653°C. Kroll (2003) has presented a discussion of the driving force during ordering and disordering processes in different forms of rate equations.

On the strength of additional experiments that are discussed below, we believe that the point defects did equilibrate at the experiments at 650°C and 750°C. Thus, in these experiments, K$^+$(ord)≈K$^+$(disord), at least within the limits of experimental errors. For the calculation of cooling rates of orthopyroxenes natural samples, it is the Arrhenian relation derived from the results of ordering experiments that is important. In order to derive the Arrhenian relation for K$^+$ (ord), we ignored the data at 580°C and K$^+$ (disord) datum 550°C, because the crystal did not achieve point defect equilibrium, but included the datum for ordering experiment at 550°C on the ground that, according to the above discussion, this datum provides an upper limit to the value of K^+ (ord) at 550°C because the sample was pre-annealed at 650°C. Linear regression of the $\ln(C_0K^+)$ versus $1/T$ for the selected data yields the following relation at fO_2 defined by the WI buffer

$$\ln(C_oK^+) = -\frac{35213(\pm 2170)}{T(K)} + 30.9(\pm 2.3)\,\mathrm{min}^{-1} \qquad (7)$$

with an activation energy of 70 (± 4.3) kcal/mol. The fitted relation to the kinetic data is illustrated in Fig. 3 as a solid line. Since K^+ (ord) at 550°C might have been somewhat overestimated, the use of the above relation would provide an upper limit to the cooling rate of natural samples. It would seem that too much weight has been placed on a single point at 550°C in the above regression. However, a second Arrhenian derived from continuous cooling experiments, which are discussed below, is almost exactly the same as the above relation.

Continuous cooling experiments: fO_2 dependence of rate constant

The quenched site occupancies in the continuous cooling experiments are listed in Table 3 along with the initial annealing temperature, T_o, closure temperature, T_c and the cooling rate or the cooling constant, depending on whether the cooling rate is constant or not, for each experiment. These data were modeled according to the method of Ganguly (1982) in which a continuous T–t path was broken up into a series of small isothermal steps and the final site occupancy in one step was treated as the initial site occupancy in the next step. The change in site occupancy for the time lapse in an isothermal step was calculated according to the transform of Eq. 1 due to Ganguly (1982; Eq. 31).

We modeled the evolution of site occupancies of the HO (Fs_{50}) samples for the continuous cooling experiments using the Arrhenian relation as given by Eq. 7. The results show that only a subset of the data can be fitted by this rate law. These are illustrated in Fig. 4 which shows calculated evolution of X^{M2}_{Fe} as a function of temperature, using the T–t data of the experiments, and comparison of the data with the quenched values of X^{M2}_{Fe}, as shown by symbols with error bars. The rest of the data can be fitted by adjusting the C_0K^+ obtained from Eq. 7 to that of QFI buffer (O'Neill 1987, 1988) according to the theoretically expected relation that (C_0K^+) varies as $(fO_2)^{1/6}$. These results are illustrated in Fig. 5.

The fact that the appropriate rate constants of the samples in the continuous cooling experiments seem to conform to fO_2 condition of either WI or QFI buffer suggests that the fO_2 condition within the sealed silica tube with a WI buffer mixture was controlled by either the buffer mixture or the interaction of metallic iron with the silica tube according to $SiO_2 + 2Fe + 1/2O_2 = Fe_2SiO_4$. The reason for this may be the inhomogeneity of the buffer mixture such that for the experiments illustrated in Fig. 5, metallic iron was preferentially concentrated near the top of the Au capsule containing the buffer mixture.

To check the above hypothesis, we conducted two additional continuous cooling experiments using (a) Au tube instead of silica tube and WI buffer mixture or (b) a silica tube and only metallic iron to control fO_2. In the first experiment, the fO_2 should conform to that of WI buffer while in the second one the fO_2 should conform to QFI buffer in the presence of metallic iron since the trapped atmosphere inside the silica tube had an initial fO_2 much greater than that of this buffer. The results of these experiments along with their simulated evolution of site occupancies as function of temperature are illustrated in Figs. 4 (sample F: HO11-109) and 5 (sample M:HO11-108), respectively. To simulate the evolution of X^{M2}_{Fe} as a function of temperature, we used C_0K^+ data for WI buffer (Eq. 7) for the sample HO11-109, whereas for simulation for the sample HO11-108, the C_0K^+ obtained from Eq. 7 was adjusted to that of QFI buffer according to $C_0K^+ \propto (fO_2)^{1/6}$. The simulated and experimentally determined values of quenched site occupancies are found to agree in both cases within the limits of experimental uncertainties. Thus, these results suggest that C_0K^+ varies approximately as $(fO_2)^{1/6}$ and also that the earlier experimental data in the presence of WI buffer mixture in sealed silica tubes clustered into two groups (Figs. 4, 5) because of development of two types of fO_2 conditions within the sealed silica tube containing WI buffer mixture. We also note from the data in Table 3 and Fig. 5 that the site occupancy determinations of the samples with around 50 mol% Fe component are not significantly affected by changing the temperature of X-ray data collection from 298 K to 110 K.

As additional tests of the dependence of (C_0K^+) on fO_2, we conducted two continuous cooling experiments in the presence of NNO buffer mixture inside sealed silica tubes. The results are illustrated in Fig. 6 along with the simulated evolutions of X^{M2}_{Fe}. The rate constants given by Eq. 7 were adjusted for the change of fO_2 condition from WI to NNO buffer (O'Neill 1987, 1988), assuming that $C_0K^+ \propto (fO_2)^{1/6}$. The very good agreement between the final values of X^{M2}_{Fe} in the simulations and experiments confirm the validity of the assumed dependence of (C_0K^+) on fO_2. The entire set of experimental data shown in Figs. 5 and 6 permits a range of value of the exponent of fO_2 from 5.5 to 6.5, i.e., $K^+ \alpha (fO_2)^n$, with $n = 5.5$–6.5. It should be noted that the T_c-s for Fe–Mg ordering in the continuous cooling experiments are ~650–700°C. The systematic fO_2 dependence of the data confirms that point defect equilibrium with fO_2 was achieved down to ~650°C in the small orthopyroxene grains (~400×250×100 μm, on the average) during the kinetic experiments.

The results for the continuous cooling experiments for the low iron samples, ST5(Fs_{16}), along with those from Ganguly and Stimpfl (2000) for orthopyroxene from the same source (Steinbach meteorite) are illus-

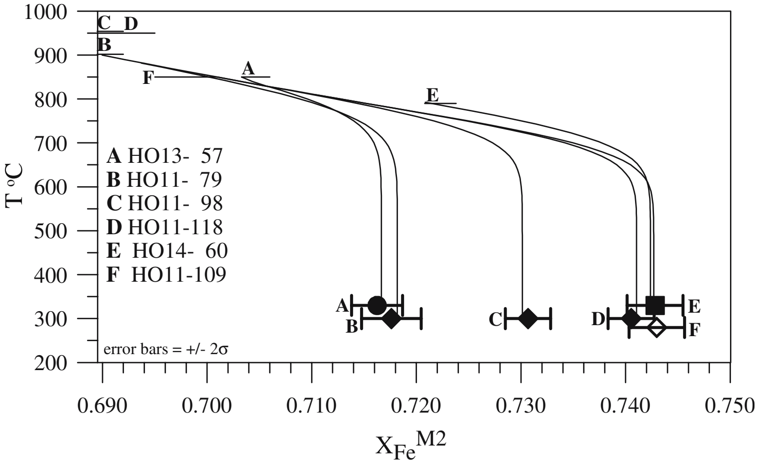

Fig. 4 Simulated evolution (*solid lines*) of $X_{\mathrm{Fe}}^{\mathrm{M2}}$ for continuous cooling experiments for HO(Fs_{50}) crystals. The fO_2 conditions were inferred to have been buffered by WI mixture buffer. The symbols show the quenched site occupancies for each experiment (Table 3), and are plotted at an arbitrary temperature below the closure temperature of Fe–Mg ordering. The *horizontal lines* above 800°C represent the initial temperature (T_0) for each experiment. *Empty diamond*: HO11-109 (F) experiment conducted in a sealed gold capsule. All others were conducted in sealed silica tube

trated in Fig. 7. The site occupancies reported in Fig. 7 for the data of Ganguly and Stimpfl (2000) (open squares) were modified according to to Stimpfl (2005a, b), keeping Mn restricted completely to the M2 site. The experiments by Ganguly and Stimpfl (2000) were conducted in the presence of a WI buffer mixture inside sealed silica tubes, whereas those in the present study were conducted in the presence of WI mixture that was sealed inside either a silica tube (filled hexagon) or Au capsule (open hexagons).

The Arrhenian parameters, ($C\mathrm{K}^+{}_0$) and Q, were retrieved by numerical simulation of T versus $X_{\mathrm{Fe}}^{\mathrm{M2}}$ paths for the different samples so that there is best statistical match between simulated and experimental values of the quenched site occupancies of all samples (Fig. 8). For this purpose, the following function was minimized.

$$M = \frac{1}{\sigma_i^2}\sum_i \left[X_{\mathrm{Fe}}(\mathrm{M2})^q_{\exp(i)} - X_{\mathrm{Fe}}(\mathrm{M2})^q_{\mathrm{sim}(i)}\right]^2, \qquad (8)$$

where $X_{\mathrm{Fe}}(\mathrm{M2})^q$ indicates the quenched value of $X_{\mathrm{Fe}}^{\mathrm{M2}}$ in either the experiment or the simulation, as specified, and σ_i is the standard deviation of an experimental value. The retrieved Arrhenian relation for ST5(Fs_{16}) is given by

$$\ln(C_o\mathrm{K}^+) = -\frac{39609(\pm 500)}{T(\mathrm{K})}\,\mathrm{min}^{-1} + 29.10(\pm 0.45) \qquad (9)$$

with an activation energy of ~79 kcal/mol. We also carried out a similar exercise to simultaneously retrieve the Arrhenian parameters from the continuous cooling experiments of the HO(Fs_{50}) samples. The results are indistinguishable from the Arrhenius relation derived from the isothermal time series experiments, Eq. 7.

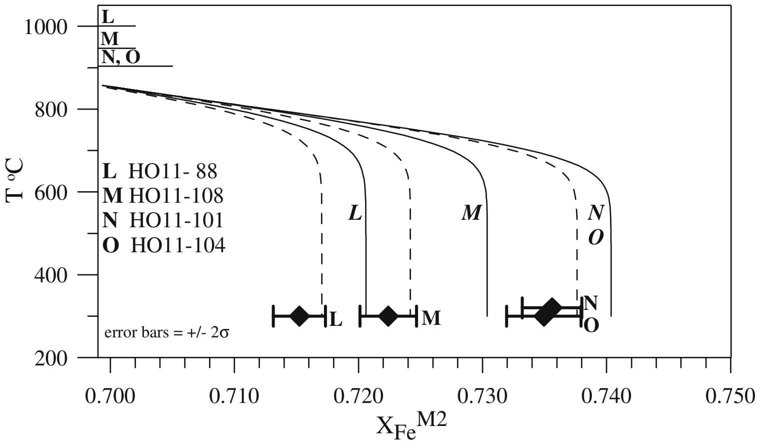

Fig. 5 Simulated evolution of $X_{\mathrm{Fe}}^{\mathrm{M2}}$ versus T using the *T–t* conditions of continuous cooling experiments for HO(Fs_{50}) crystals along with (a) kinetic constants derived from the isothermal ordering experiments at fO_2 of WI buffer, Eq. 7 (*solid lines*), and (b) adjusted values of the kinetic constants to fO_2 of QFI buffer assuming that $\mathrm{K}^+ \propto (fO_2)^{1/6}$ (*dashed lines*). HO11-108 (M) experiment was conducted in a sealed silica tube with Fe powder, only

Fig. 6 Simulated evolution of X_{Fe}^{M2} versus T using the T–t conditions of continuous cooling experiments of HO(Fs_{50}) crystals at NNO buffer. The evolution of the site occupancies were computed using the kinetic constants derived from Eq. 7 that is valid for fO_2 condition of WI buffer and adjusting them to the fO_2 of NNO buffer according to $K^+ \propto (fO_2)^{1/6}$

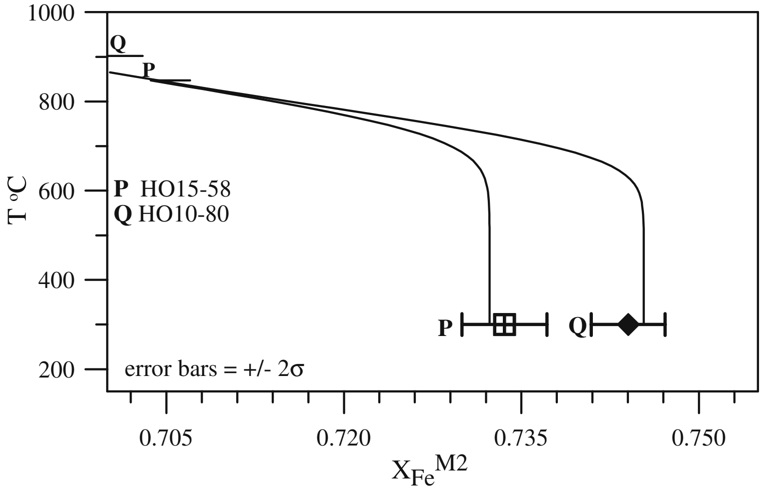

The success in modeling all data simultaneously including that in which the buffer and sample were sealed together in an Au capsule indicates that the fO_2 conditions of the continuous cooling experiments using the ST samples were controlled by the WI buffer equilibrium. The rate constant derived by Ganguly and Stimpfl (2000) is larger than that given by Eq. 9 by about 0.3 log units. This difference is due to the different schemes of partitioning Mn between the M2 and M1 sites, as discussed above.

Compositional dependence of kinetic constants

From the data collected for the intermediate (HO) and low iron (ST) samples, we generated a calibration for $\ln C_0K^+$ that takes into account both the temperature and the compositional dependence of the kinetic constants. Because the two calibrations showed different values for both activation energy and K_o, we treated both parameters as function of composition. Following earlier studies on the compositional dependence of interdiffusion and order–disorder kinetics (Morioka and Nagasawa 1991; Ganguly and Tazzoli 1994), it was assumed that $\ln(C_0K^+)$ changes linearly with X_{Fe}. However, it is emphasized that the linear relation should not be extrapolated much beyond the bounds of the experimental data, $X_{Fe} \sim 0.16$–0.50. A stepwise statistical analyses of the kinetic data were performed using the code SPSS (12.0). This procedure yielded the following Arrhenian relation for the forward rate constant (C_0K^+) at the WI buffer:

$$\ln(C_oK^+) = -\frac{41511 - 12600X_{Fe}}{T(\mathrm{K})} + 28.26 + 5.27X_{Fe}\,\mathrm{min}^{-1}. \tag{10}$$

The temperature and compositional dependence of the rate constant, as expressed by the above equation, is illustrated in Fig. 8 for the chosen orthopyroxene compositions and compared with the results from the optimized relation that was derived by Ganguly and Tazzoli (1994) from a critical selection of the available experimental data. It is evident that Eq. 10 yields a stronger compositional dependence and considerably smaller value of K^+ at any temperature than those

Fig. 7 Simulated evolution of X_{Fe}^{M2} versus T at fO_2 condition of WI buffer using the T–t conditions of cooling experiments for orthopyroxene crystals separated from the Steinbach meteorite. Sample ST5: this work, for which the quenched site occupancies are shown by *hexagons*. *Open squares*: data from Ganguly and Stimpfl (2000) modified according to Stimpfl (2005a, b)

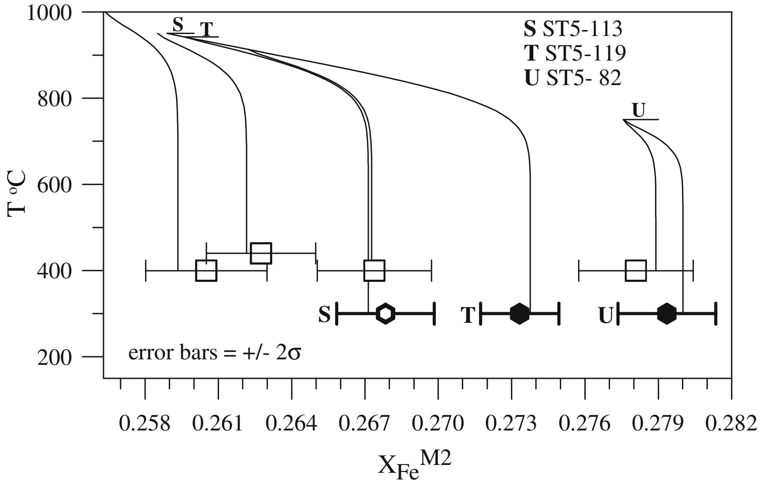

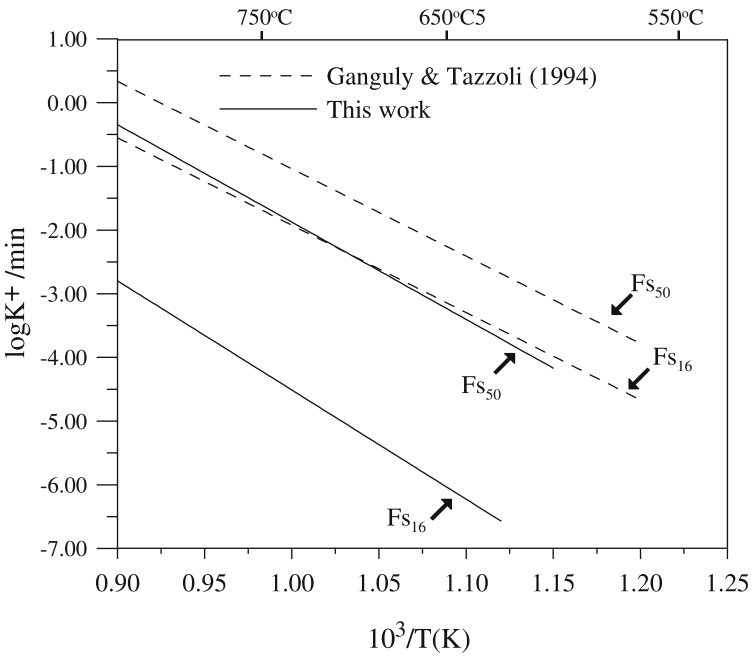

Fig. 8 Comparison of the log K^+ versus $1/T$ relation, according to Eq. 10, for orthopyroxene compositions of Fe_{16} and Fs_{50}, which were used in the present experimental studies, with those calculated from the optimized relation of Ganguly and Tazzoli (1994) for the same compositions

obtained from the optimized relation of Ganguly and Tazzoli (1994). The reason for this difference is not clear.

Application of the kinetic data to Central Gneiss Complex, British Columbia

Using the age data of a number of decay systems with different closure temperatures spanning a range of ~200°C to 700°C, Hollister (1982) constrained the temperature–time (T–t) path of exhumation of the granulites from the Khtada Lake metamorphic complex (KLMC) that lies within the Central Gneissic Complex (CGC) of British Columbia (Fig. 9), and which is also the source of the HO(Fs_{50}) samples used in this study. In order to illustrate the application of the Fe–Mg ordering state of natural orthopyroxene crystal to retrieve the cooling rate of host rocks, we have determined the cooling rate of KLMC. Since the cooling rate of this complex seems to be well constrained from geochronological data, this specific application also provides a test for the validity of the kinetic and thermodynamic data on intra-crystalline Fe–Mg fractionation that we have determined in this study and in Stimpfl et al. (1999), respectively. We determined the intracrystalline cation fractionation of eight orthopyroxene crystals by single crystal X-ray diffraction and structure refinement, as described above. These data are summarized in Table 4. Using Eq. 5, which represents a calibration of temperature dependence of Fe–Mg ordering in the orthopyroxene crystals separated from the same rock sample, these data yielded a narrow range of closure temperature of ordering, T_C, of 283–294°C, with an average of 288°C.

As illustrated in Fig. 9, there are two distinct segments in T–t data of Hollister (1982) for KLMC, namely a high-temperature segment indicating rapid cooling at a rate of ~100°C/Myr between 700°C and 300°C, and a low-temperature segment indicating much slower cooling, at a rate of ~15°C/Myr. As discussed by Ganguly (1982), the cooling rate obtained from the data on cation ordering reflects the cooling rate around T_C. Thus, we expect that the cation ordering data would primarily reflect the slow cooling rate below 300°C.

We have simulated the evolution of Fe–Mg ordering in orthopyroxene from KLMC assuming that the T–t path followed an "asymptotic law" $1/T(\mathrm{K}) = 1/T_o + \eta t$ (Dodson 1973; Ganguly 1982), where T_o is the initial temperature (in K) and η is a time constant with the dimension of $K^{-1}\ t^{-1}$. It was shown by Ganguly (1982) that the cooling rate at the T_c is quite insensitive to the choice of cooling model; the difference between the models are reflected in the calculation of cooling rates above and below T_c. We assumed a T_o of 400°C and fO_2 between QFM and NNO buffers, which is a reasonable assumption for the fO_2 of granulite facies rocks (Lappin and Hollister 1980). As discussed by Ganguly (1982), the calculation of cooling rate is not sensitive to the choice of T_o as long as it is within the domain where thermodynamic equilibrium is maintained during cooling.

The expression for the specific rate constant, (C_oK^+), as derived from the kinetics experiment at WI buffer, Eq. 7, was corrected for the effect of fO_2 according to $K^+ \propto (fO_2)^{1/6}$. The fO_2 versus T data for the WI, QFM and NNO buffers were taken from O'Neill (1987, 1988). Following the same procedure as discussed for the modeling of quenched site occupancies in continuous cooling experiments we calculated the evolution of site

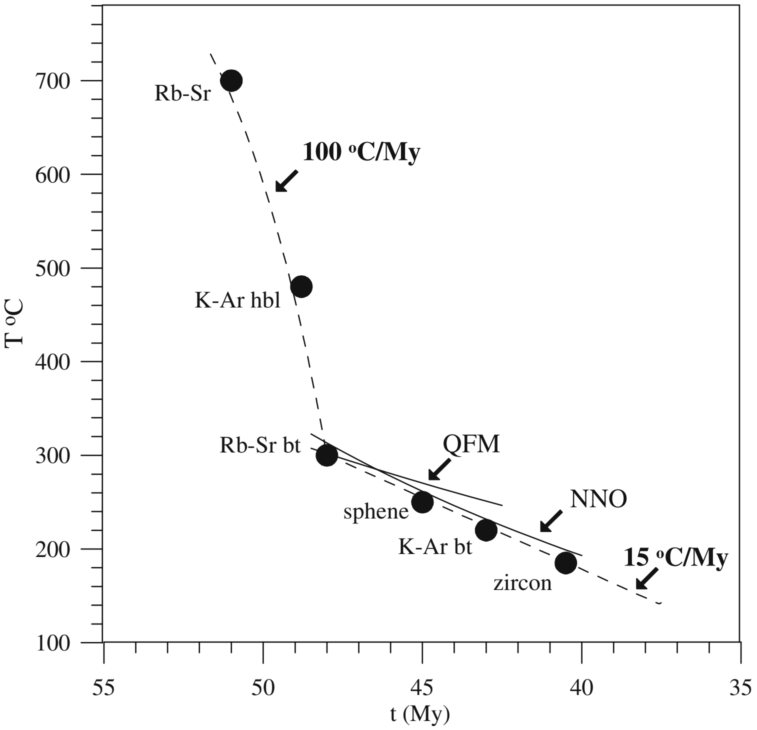

Fig. 9 Closure temperature versus age of different geochronological systems from the Central Gneissic Complex, Canada (Hollister 1982) showing a two stage cooling. The *T–t* paths retrieved from the Fe–Mg ordering data for fO_2 defined by QFM and NNO buffers are shown as *solid lines*

Table 4 Summary of the site occupancy data, and k_D of the orthopyroxene crystals from the KLMC, sample TPR-30F (HO)

	HO8	HO10	HO11	HO13	HO14	HO15	HO28	HO39B
M2 site								
Mg	0.096 (1)	0.104 (1)	0.104 (1)	0.103 (1)	0.102 (1)	0.104 (1)	0.095 (1)	0.089 (1)
Fe^{2+}	0.851	0.849	0.846	0.846	0.845	0.845	0.853	0.859
Mn	0.015	0.015	0.015	0.015	0.014	0.015	0.014	0.015
Na	0.001	0.000	0.001	0.000	0.001	0.001	0.000	0.001
Ca	0.037	0.031	0.034	0.036	0.038	0.035	0.038	0.036
M1 site								
Mg	0.860 (1)	0.864 (1)	0.867 (1)	0.865 (1)	0.856 (1)	0.865 (1)	0.852 (1)	0.855 (1)
Fe^{2+}	0.117	0.114	0.110	0.114	0.120	0.114	0.126	0.129
Al	0.019	0.020	0.020	0.018	0.019	0.018	0.017	0.012
Ti	0.004	0.002	0.003	0.003	0.004	0.003	0.004	0.004
T site								
Si	1.974	1.975	1.974	1.976	1.974	1.976	1.975	1.981
Al	0.026	0.025	0.026	0.024	0.026	0.024	0.025	0.019
k_D	0.0154 (3)	0.0162 (4)	0.0157 (3)	0.0161 (4)	0.0170 (4)	0.0162 (3)	0.0165 (3)	0.0158 (3)

The Esd for the site occupancies of Fe and Mg arising from those of structural data, as given by the refinement program RFINE90. Errors from chemical analyses combined with those from the structural refinement approximately doubles the Esd

occupancies as a function of temperature during cooling for the orthopyroxene crystals from KLMC. For the kinetic constant adjusted for fO_2 of QFM buffer, a value of $\eta = 3.4\times10^{-5}$ K^{-1} $(My)^{-1}$ was found to yield quenched site occupancies that matched the observed values of all crystals within their ±2σ error limits. For NNO buffer, the equivalent value of η is 5.4×10^{-5} K^{-1} $(My)^{-1}$. The simulated evolution of X_{Fe}^{M2} versus temperature for the different crystals, using kinetic constant adjusted to fO_2 of QFM buffer, are illustrated in Fig. 10. The simulations are found to follow the equilibrium paths down to ~ 300°C, which implies that the quenched ordering states do not have any memory of cooling rate above this temperature. The retrieved values of η imply cooling rate (given by $-\eta T^2$) of ~11–17°C/Myr at T_c(ord) of 288°C. The *T–t* paths according to the asymptotic cooling model are shown in Fig. 9. There are significant uncertainties in the closure temperatures of geochronological systems arising from variations of grain size, cooling rate and matrix phases (Ganguly and Ruiz 1986; Ganguly and Tirone 1999). Nonetheless, the cooling rates obtained from the quenched Fe–Mg ordering states of orthopyroxene are in good agreement with the geochronological constraints below 300°C.

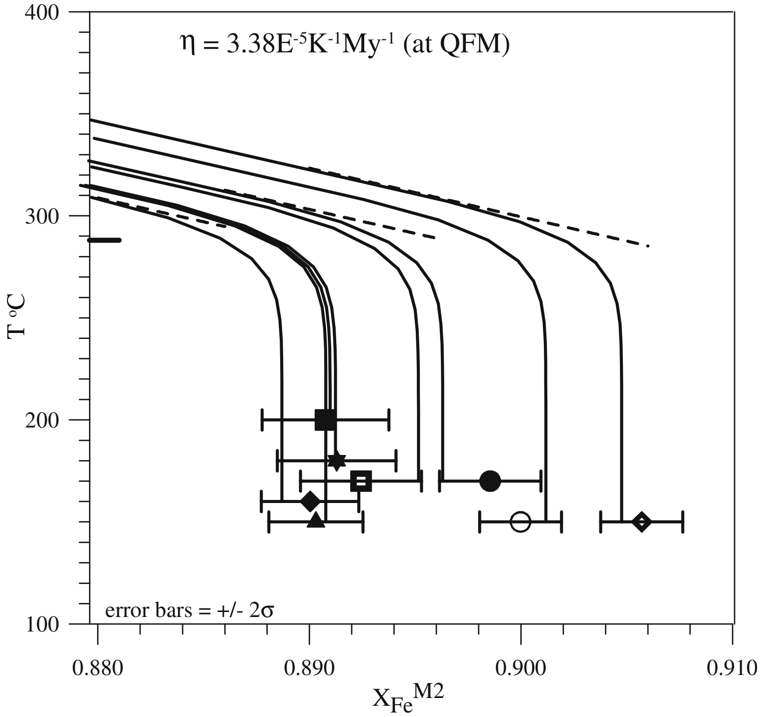

Fig. 10 Simulated evolution of $X_{\mathrm{Fe}}^{\mathrm{M2}}$ versus *T* at fO_2 condition of QMF buffer using the kinetic constants from Eq. 7 for the natural samples from the Central Gneiss Complex. *Symbols* are the observed site occupancies. The *horizontal line* at 288°C represents the average T_c for the HO samples

Acknowledgements This research was supported by NASA grants NAG5-10486 and NNG04GG26G. The single crystal X-ray diffraction studies were carried out in the X-ray laboratory of the Department of Chemistry, University of Arizona. The CCD equipped Area detector was purchased with an NSF grant CHE-9610374. We are grateful to Dr. M. Carducci for his help in using the X-ray equipments and the software for data reduction. Thanks are due to Prof. Chiara Domeneghetti and an anonymous reviewer for careful reviews constructive suggestions that led to significant improvement of the analysis of the data and clarity of presentation, to Prof. Hans Annersten for the Mössbauer analysis of orthopyroxene, and Prof. Linc Hollister for the KLMC samples. The senior author acknowledges helpful discussions with Dr. Robert P. Ilchik.

References

Anovitz LM, Essene EJ, Dunham WR (1988) Order-disorder experiments on orthopyroxenes: implication for the orthopyroxene geospeedometer. Am Mineral 73:1060–1073

Besancon JR (1981) Rate of cation disordering in orthopyroxenes. Am Mineral 66:965–973

Blessing RH (1987) Data reduction and error analysis for accurate single crystal diffraction intensities. Crystallogr Rev 1:3–58

Bruker (1997a) SAINT reference manual Version 5. Bruker AXS Inc. Madison, Wisconsin, USA

Bruker (1997b) SMART reference manual Version 5. Bruker AXS Inc. Madison, Wisconsin, USA

Buening DK, Buseck PR (1973) Fe-Mg lattice diffusion in olivine. J Geophys Res 78:6852–6862

Càmara F, Doukhan JC, Domeneghetti MC, Zema M (2000) A TEM study of Ca-rich orthopyroxene with exsolution products: implication for Mg–Fe ordering process. Eur J Mineral 12:735–748

Dodson MH (1973) Closure temperature in cooling geological and petrological systems. Cont Min Pet 40:259–274

Dollase WA, Newman WI (1984) Statistically most probable stoichiometric formulae. Am Mineral 69:553–556

Finger LW, Prince E (1975) A system of FORTRAN IV computer programs for crystal structural computations. NBS Tech Notes 854

Ganguly J (1982) Mg-Fe order-disorder in ferromagnesian silicates: II. Thermodynamics, kinetics and geological applications. In: Saxena SK (ed) Advances in physical geochemistry, 2. Springer, Berlin Heidelberg New York, pp 58–99

Ganguly J, Domeneghetti MC (1996) Cation ordering of orthopyroxene from the Skaegaard intrusion: implication for the subsolidus cooling rates and permeabilities. Contrib Mineral Petrol 122:359–367

Ganguly J, Ruiz J (1986) Time-temperature relation of mineral isochrons: a thermodynamic model, and illustrative examples for the Rb–Sr system. Earth Planet Sci Let 81:338–34

Ganguly J, Stimpfl M (2000) Cation ordering in orthopyroxenes from two stony iron meteorites: implications for cooling rates and metal-silicate mixing. Geochim Cosmochim Acta 64:1291–1297

Ganguly J, Tazzoli V (1994) Fe^{2+}-Mg interdiffusion in orthopyroxene: Retrieval from the data on intracrystalline exchange reaction. Am Mineral 79:930–937

Ganguly J, Tirone M (1999) Diffusion closure temperature and age of a mineral with arbitrary extent of diffusion: theoretical formulation and applications. Earth Planet Sci Let 170:131–140

Ghose S (1962) The nature of Mg^{2+}-Fe^{2+} distribution in some ferromagnesian silicate minerals. Am Mineral 47:338–394

Hawthorne FC, Ito J (1978) Refinement of the crystal structures of $(Mg_{0.776}Co_{0.224})SiO_3$ and $(Mg_{0.925}Mn_{0.075})SiO_3$. Acta Crystall B34:891–893

Heinemann R, Kroll H, Langenhorst F, Lueder T (2000) Time and temperature variation of the intracrystalline Fe^{2+}, Mg fractionation in Johnstown meteoritic orthopyroxene. Eur J Mineral 12:163–176

Hollister LS (1982) Metamorphic evidence for rapid (2 mm/yr) uplift of a portion of the Central Gneiss Complex, Coast Mountains, B.C. Can Mineral 20:319–331

Kroll H (2003) Rate equations for non-convergent order-disorder processes—a review and application to orthopyroxene. Eur J Min 15:7–19

Kroll H, Lueder T, Schlenz H, Kirfel A, Vad T (1997) The Fe^{2+}, Mg distribution in orthopyroxene: a critical assessment of its potential as a geospeedometer. Eur J Mineral 9:705–733

Lappin AR, Hollister LS (1980) Partial melting in the Central Gneiss Complex near Prince Rupert, British Columbia. Am J Sci 280:518–545

Marais S, Salie EKH (1991) Derivation of a rate law for non-uniform systems and continuous order parameters. J Phys Condens Mat 3:3667–3670

Meisner DJ (1974) Cationic diffusion in olivine to 1400°C to 35 kb. In: Hoffmann AW, Giletti BJ, Yoder HS Jr, Yund RA (eds) Geochemical Transport and Kinetics. Carnegie Institution of Washington Publication 634, pp 117–129

Morioka M, Nagasawa H (1991) Ionic diffusion in olivine. In: Ganguly J (ed) Diffusion, atomic ordering, and mass transport: advances in physical chemistry. Springer, Berlin Heidelberg New York, 8:176–197

Mueller RF (1967) Model for order-disorder kinetics in certain quasi-binary crystals of continuously variable composition. J Phys Chem Solids 28:2239–2243

Mueller RF (1969) Kinetics and thermodynamics of intracrystalline distributions. Mineral Soc Amer Spec Pap 2:83–93

North ACT, Phillips DC, Scott MF (1968) A semi-empirical method of absorption correction. Acta Crystall A24:351–359

O'Neill HStC (1987) Free energies of formation of NiO, CoO, Ni_2SiO_4 and Co_2SiO_4. Am Mineral 72:280–291

O'Neill HStC (1988) System Fe-O and Cu-O: thermodynamic data for the equilibria Fe-"FeO", Fe-Fe3O_4, "FeO"-Fe_3O_4-Fe_2O_3, and Cu-Cu_2O, and Cu_2O-CuO form emf measurements. Am Mineral 73:470–486

O'Neill HStC (1994) Kinetics of cation order-disorder in $MgFe_2O_4$ spinel. In: Putnis A (ed) European Science Foundation Program on Kinetic Processes in Minerals and Ceramics. Cambridge, London

Saxena SK, Tazzoli V, Domeneghetti MC (1987) Kinetics of Fe^{2+}-Mg distribution in Aluminous orthopyroxene. Phy Chem Min 15:140–147

Saxena SK, Domeneghetti MC, Molin GM, Tazzoli V (1989) X-ray diffraction study of Fe-Mg order-disorder in orthopyroxene. Some kinetics results. Phy Chem Min 16:421–427

Seifert FA, Virgo D (1973) Kinetics of the Fe-Mg order-disorder reaction in Antophyllites: quantitative cooling rates. Science 188:1107–1109

Sha LK, Chappell BW (1996) Two-site multi-cation ordering-disordering in minerals: an alternative kinetic model. Am Mineral 81:881–890

Sheldrick GM (1996) SADABS. Siemens Area Detector Absorption Software. University of Gottingen. Germany

Skogby H (1992) Order-disorder kinetics in orthopyroxene of ophiolite origin. Contrib Mineral Petrol 109:471–478

Skogby H, Annersten H, Domeneghetti MC, Molin GM, Tazzoli V (1992) Iron distribution in orthopyroxene: a comparison of Mössbauer spectroscopy and X-ray refinement results. Eur J Mineral 4:441–452

Stimpfl M (2005a) Mn, Mg intracrystalline exchange reaction in donpeacorite ($Mn_{0.54}Ca_{0.03}Mg_{1.43}Si_2O_6$) and its relation to the fractionation behavior of Mn in Fe, Mg-orthopyroxene. Am Mineral 90:155–162

Stimpfl M (2005b) Erratum: Mn, Mg intracrystalline exchange reaction in donpeacorite ($Mn_{0.54}Ca_{0.03}Mg_{1.43}Si_2O_6$) and its relation to the fractionation behavior of Mn in Fe, Mg-orthopyroxene. Am Mineral 90:776

Stimpfl M, Ganguly J, Molin G (1999) Fe^{2+}-Mg order-disorder in orthopyroxene: equilibrium fractionation between the octahedral sites and thermodynamic analysis. Contrib Mineral Petrol 136:297–309

Sykes-Nord J, Molin GM (1993) Mg-Fe order-disorder reaction in Fe-rich orthopyroxene. Structural variation and kinetics. Am Mineral 921–931

Zema M, Domeneghetti MC, Molin GM, Tazzoli V (1997) Cooling rates of diogenites: a study of Fe^{+2}-Mg ordering in orthopyroxene by single-crystal x-ray diffraction. Met Planet Sci 32:855–862

Zema M, Domeneghetti MC, Tazzoli V (1999) Order-disorder kinetics in orthopyroxene with exsolution products. Am Mineral 84:1895–1901